ELSEVIER

Ultramicroscopy 57 (1995) 103–111

ultramicroscopy

Structure of planar defects in $(Sr_{0.9}Ca_{0.3})_{1.1}CuO_2$ infinite-layer superconductors by quantitative high-resolution electron microscopy

H. Zhang [a], L.D. Marks [a], Y.Y. Wang [a], H. Zhang [a,1], V.P. Dravid [a], P. Han [b], D.A. Payne [b]

[a] *Department of Materials Science and Engineering, and Science and Technology Center for Superconductivity, Northwestern University, Evanston, IL 60208, USA*

[b] *Department of Materials Science and Engineering, and Science and Technology Center for Superconductivity, University of Illinois at Urbana-Champaign, Urbana, IL 61801, USA*

Received 27 April 1994; in final form 19 August 1994

Abstract

Planar defects in the infinite-layer $(Sr_{1-x}Ca_x)_yCuO_2$ structure are believed to be responsible for superconductivity with T_c up to 110 K. In this work we present χ^2 minimization results to best fit a set of through-focal HREM images of such defects. Optimized atomic positions of the defect with an error bar of about 0.1 Å are determined. The experimental parameters for simulated defect images such as sample thickness and objective lens defocus are determined by χ^2 fitting of the corresponding experimental HREM images of the matrix.

1. Introduction

For some years the qualitative comparison of experimental-simulated HREM images based on estimated experimental parameters to validate a proposed atomic structure model has been extensively used. In the last few years, with the increasing availability of faster computers some efforts have been made towards quantitative determination of atomic structures [1–4], especially defect structures. Several different approaches to quantification of high-resolution electron microscopy have been proposed such as least-squares optimization [4,5] and the maximum entropy method which combines image plane and diffraction pattern information [6,7]. Some progress has been achieved but there are few reports of atomic position refinement by quantitative HREM.

Superconductivity with T_c up to 110 K in the simple infinite-layer $(Sr_{1-x}Ca_x)_yCuO_2$ structure, CuO_2 sheets separated by Sr and Ca cations, was first observed by Azuma et al. [8] and Hiroi et al. [9]. A significant density of planar defects was found in this system and they are believed to be responsible for the superconductivity. By combining the results of quantitative nano-probe X-ray microanalysis and through-focal HREM images a

[1] Current address: LSI Logical Co.

SSDI 0304-3991(94)00142-1

$Sr_3O_{2\pm x}$ block structural model of the defects instead of the cation deficiency model suggested by Hiroi et al. [9] has been proposed by H. Zhang et al. [10]. Here we report details of the quantitative analysis of our atomic structure model of the planar defects in $(Sr_{0.9}Ca_{0.3})_{1.1}CuO_2$ by χ^2 fitting of through-focal HREM images. An optimized atomic structure model has been obtained.

2. Experimental

Infinite-layer samples with the nominal chemical formula $(Sr_{1-x}Ca_x)_yCuO_2$ ($x = 0$, 0.3, $y = 0.9$, 1.0 and 1.1) were prepared using solid-state-synthesized low-pressure forms of $(Sr_{1-x}Ca_x)CuO_2$ with additions of CuO, followed by high-pressure oxygenation treatment. The typical synthesis parameters were: 6 GPa pressure in a classical piston-cylinder pressure at a temperature of 1050°C for about one hour. A TEM thin foil was prepared by conventional techniques, i.e. mechanical thinning followed by dimpling and ion milling. Through-focal HREM images with 10 nm focal step were obtained on a 300 kV Hitachi H-9000 microscope. Experimental images were digitized to 8 bits using an Optronics P1000 microdensitometer. The microdensitometer has been calibrated and shows a linear response to the contrast in the dynamic range of our HREM images [11]. HREM image simulations were carried out using the NUMIS software developed at Northwestern University and these were quantitatively compared against the experimental images using conventional χ^2 minimizations with SEMPER software on Apollo workstations.

3. Results

3.1. χ^2 fitting algorithm

The reduced χ^2 factor which was used for quantitative analysis of the images is defined as:

$$\chi^2 = \Sigma\left\{\left[I_e(r) - I_c(r)\right]^2/\sigma_e^2(r)\right\}/(N-M), \quad (1)$$

where $I_e(r)$ and $I_c(r)$ are the experimental and calculated images, $\sigma_e(r)$ the standard deviation of the experimental images, N the total number of pixels in the image and M the number of parameters that are varied.

If we consider only the statistical error due to electron shot noise the standard deviation σ_e can be estimated as $\sqrt{I_e}$, where I_e is the total number of electrons per pixel in the images. However, in addition to electron shot noise, many factors such as ion and electron beam damage, thin layers of amorphous material on the surfaces of the sample, strain fields both intrinsic and those produced by the sample preparation and so on will affect the experimental images. Therefore the standard deviation σ_e for the calculation of χ^2 was determined from local variations in the experimental data to take account of all these, using direct calculations with up to 12 different values for 64×64 pixel^2 (8.32 Å $\times$ 8.32 Å) regions to get the average value of the standard deviation.

To compare the absolute intensity of the experimental and simulated images the simulated image was scaled to the experimental image by multiplying by the mean of intensity of the experimental image, i.e.

$$I_c(r) = I_c(r)\ I_e(\text{mean})/I_c(\text{mean}). \quad (2)$$

A χ^2 equal to 1 is considered to be a good fit for the structure model, i.e. the difference between experimental and simulated images is comparable with the uncertainty of the experiment.

3.2. Determination of the experimental parameters by fitting the infinite-layer matrix

Fig. 1 is a low-magnification HREM image along [100] direction of $(Sr_{0.7}Ca_{0.3})_{1.1}CuO_2$ infinite-layer matrix showing the typical morphology. A significant density of planar defects perpendicular to the c axis of the infinite-layer matrix are randomly distributed in the matrix.

Fig. 2 is a set of through-focal HREM images of the infinite-layer compound and these planar defects. The simulated images which are digitally pasted (with absolute values) are shown in the

figure as inserts. The contrast and configuration of the defects varied a lot with the defocus. The bright spots in defect region in Fig. 2a at a defocus of 0 Å determined by χ^2 shown later reverse contrast to dark spots in Fig. 2b at a defocus of −460 Å and come back to bright spots in Fig. 2c at a defocus of −740 Å.

The structure of the infinite-layer compound $(Sr_{0.9}Ca_{0.3})_{1.1}CuO_2$ consists of planar CuO_2 sheets separated by single cation Sr and Ca. A tableau of HREM images based on the structure model was calculated and by comparison with the experimental images and combining the value of the through-focal steps the objective lens defocus and sample thickness were roughly estimated as about 0, −400 and −700 Å defoci for Figs. 2a, 2b and 2c, respectively, and the thickness as 15 to 35 Å since the area of the images are very close to the edge of the sample. χ^2 fitting was carried out for more accurate values.

Fig. 3 illustrates the change of χ^2 as a function of the sample thickness for the three different images, 0, −460 and −740 Å defoci, respectively. For the defoci −460 Å and −740 Å the thick-

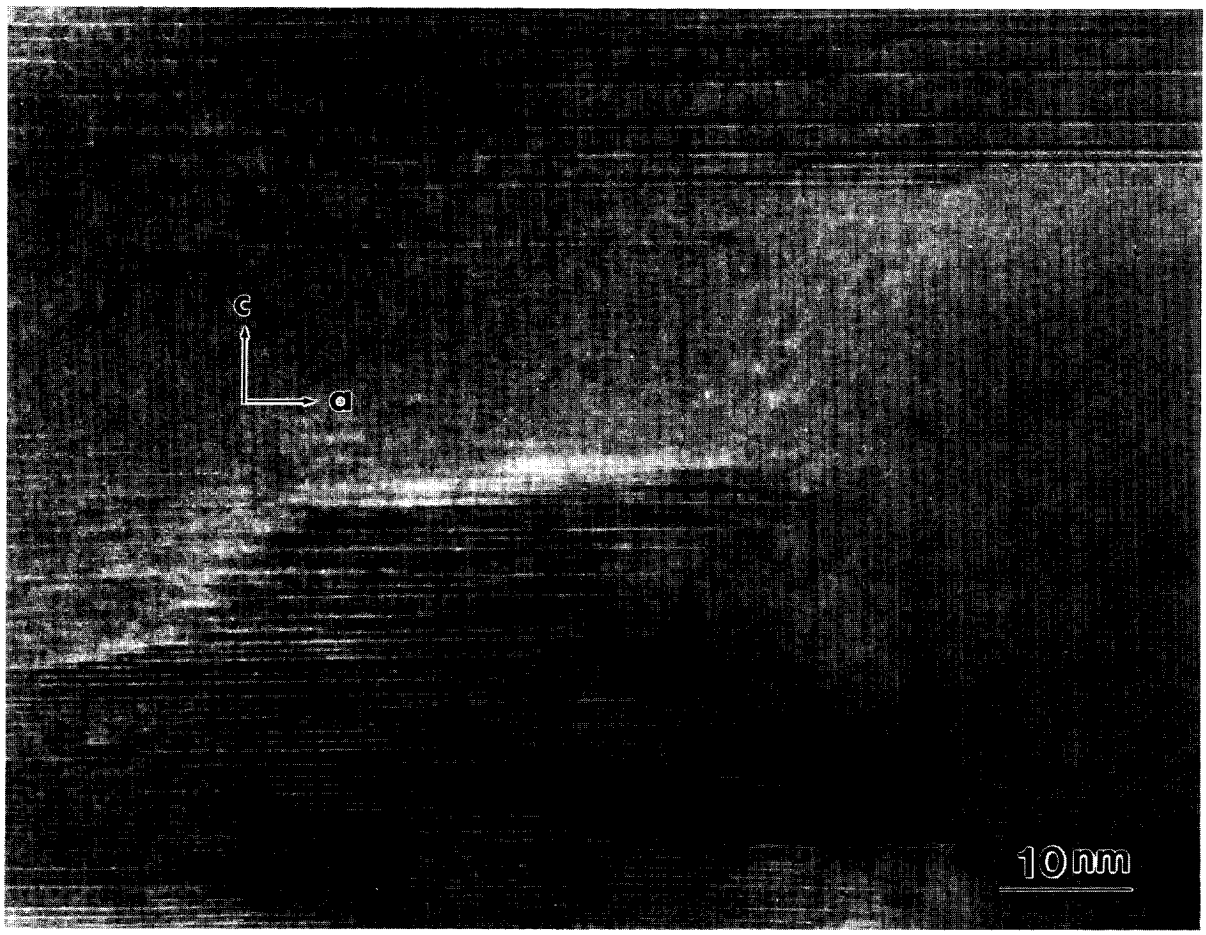

Fig. 1. Low-magnification HREM image of the $(Sr_{0.9}Ca_{0.3})_{1.1}CuO_2$ infinite-layer compound showing a significant density of the planar defects.

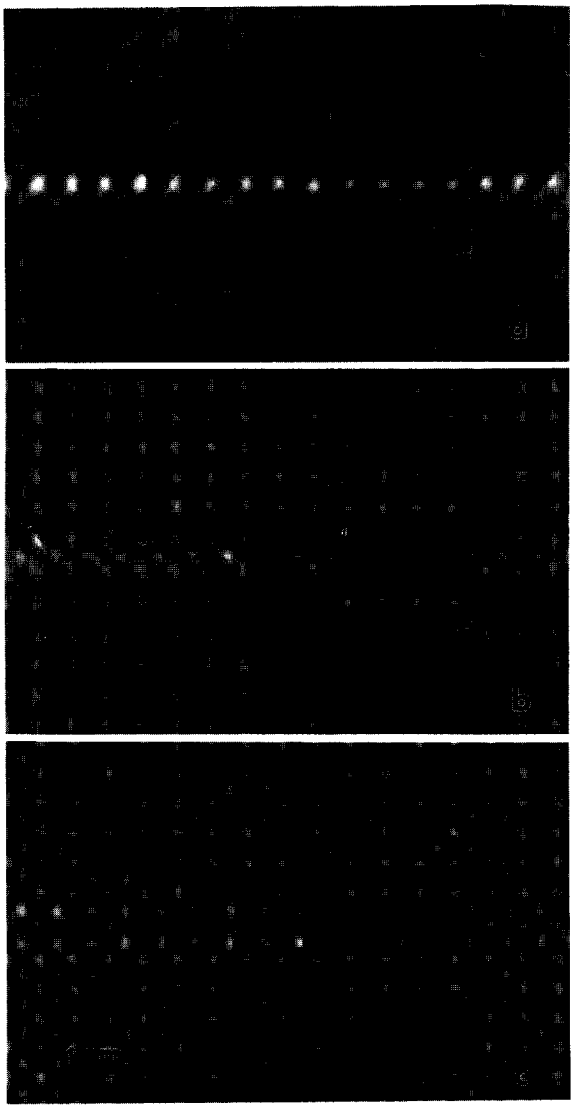

Fig. 2. Experimental and digitally pasted simulated HREM images of the planar defects in the infinite-layer compounds as a function of objective lens defocus. The defoci are 0 Å, −460 Å and −740 Å for (a), (b) and (c), respectively, with a sample thickness about 20 Å.

ness is 20 ± 2 Å but for the 0 focal image the thickness is below 15 Å which is not reasonable. Since almost the same area was selected for the fitting 20 Å was used for all the image analysis.

The variation of χ^2 as a function of the defocus with the thickness of 20 Å is shown in Fig. 4 for the three images. In Fig. 4b there is a region in which χ^2 only slightly varied with the defocus which makes it difficult to precisely fit the right focus. This is predictable for a defocus close to

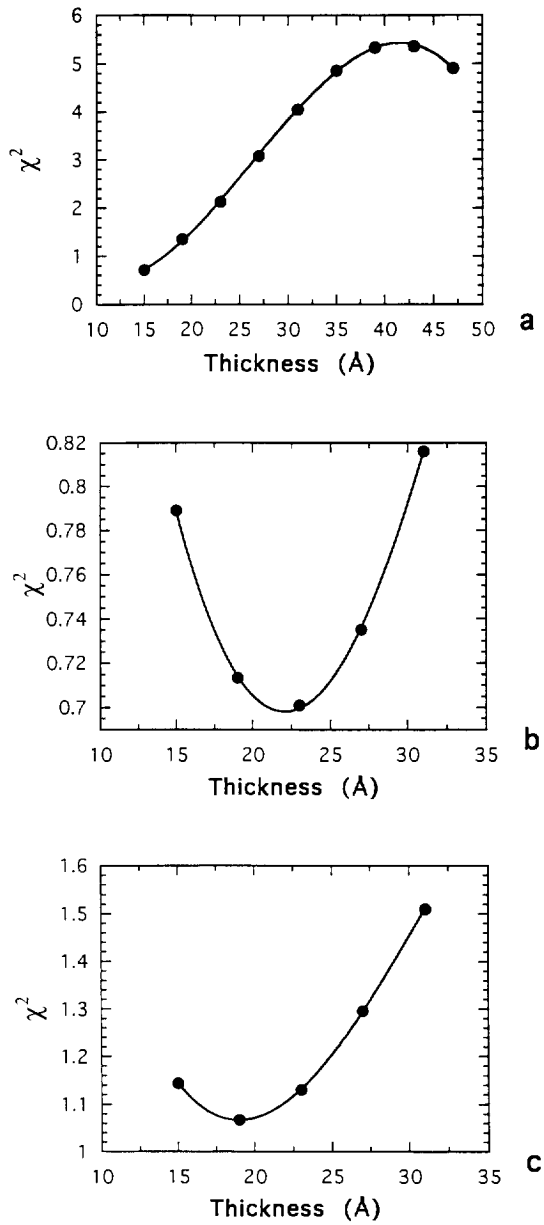

Fig. 3. The variation of χ^2 as a function of the sample thickness for the three different defoci, (a) 0 Å, (b) −460 Å and (c) −740 Å.

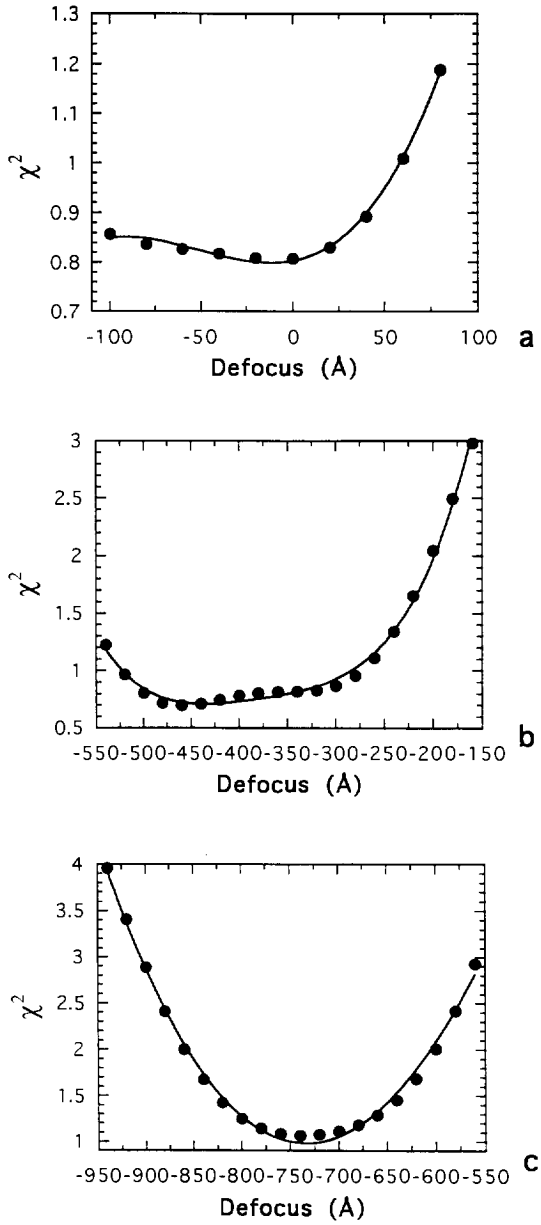

Fig. 4. The change of χ^2 as a function of the defoci with a thickness of 20 Å for three images, (a) Fig. 2a, (b) Fig. 2b and (c) Fig. 2c, respectively.

Scherzer. The defoci at the smallest χ^2, 0, -460 and -740 Å for Figs. 4a, 4b and 4c, respectively, were used for further calculation. It is interesting to note that the configuration for Figs. 4a, 4b and 4c are quite different which reflect the response of the images to variation of the defocus. χ^2 is also less sensitive to the sample thickness at a defocus close to Scherzer.

It should be pointed out that vibration (rms) was added to the simulated images as a Gaussian distribution with radius 5.4 pixels for images at 0 and -460 Å defocus, 4.5 pixels for the image at -740 Å defocus. 5.4 pixels and 4.5 pixels correspond to 0.70 Å and 0.59 Å, respectively, in our case which is very likely from the sample vibration when the images were taken. Fig. 5 shows the change of χ^2 as a function of vibration for the image at -740 Å defocus. A minimum χ^2 position has been obtained at a vibration of 4.5 pixels. Similar phenomena were present for the images at defoci 0 Å and -460 Å. The effect of the vibration on the structure refinement will be discussed later.

Since there are so many variables in the fitting in some cases overfitting cannot be avoided such as in Figs. 3a and 3b. The values at the smallest χ^2 were chosen for further calculation.

The parameters of convergence and energy spread used in our simulations were 1.2 mrad and 100 Å which are typical values under the condition of the operation. These values were also confirmed by comparing the power spectra from

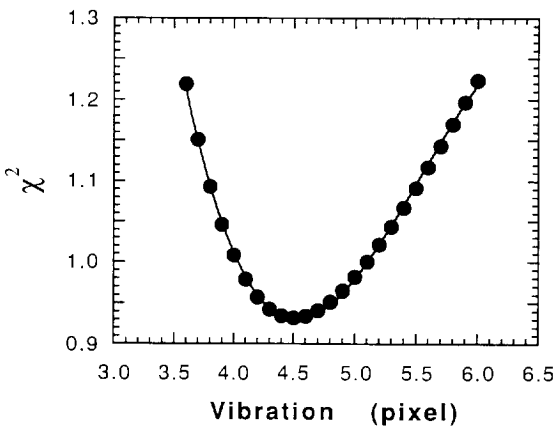

Fig. 5. The change of χ^2 as a function of vibration for the image of Fig. 2c. The vibration is expressed by radius in pixels of a Gaussian.

the amorphous edge in HREM images against the simulated CTF for all the different defoci. The spherical aberration constant C_s is 0.9 mm. Here we assume that the astigmatism, beam tilt and crystal tilt are zero which is acceptable from the quality of the images.

3.3. Structure refinement of the defect model

Using the microscope parameters described in the previous section we now consider the atomic positions of the structure model of the defect shown in Fig. 6. Since a significant depletion of Ca in the defect region was observed by quantitative X-ray microanalysis [10], a $Sr_3O_{2\pm x}$ block model for the defects without Ca was used. The structure model represents the substitute of an $Sr_3O_{2\pm x}$ block for a Sr(Ca)–CuO_2–Sr(Ca) block in an otherwise infinite-layer structure. The middle layer consists of a stoichiometric Sr–O sheet while the other Sr–O layers adjacent to the CuO_2 sheets of the infinite-layer compound have about 50% occupancy of oxygen based on charge neutrality arguments. Therefore, the strontium atoms within the middle layer are not co-planar, i.e. they are staggered up and down within the respective layers due to these oxygen atoms. About 50% occupancy of oxygen at the possible sites in the first and third Sr–O layers leads to apical oxygen atoms for 50% of the copper ions in the adjacent CuO_2 planes which are believed to be important in the superconductivity of these cuprate compounds. The 50% occupancy of oxygen was assumed to be random within the first and the third Sr–O layers for the image simulations.

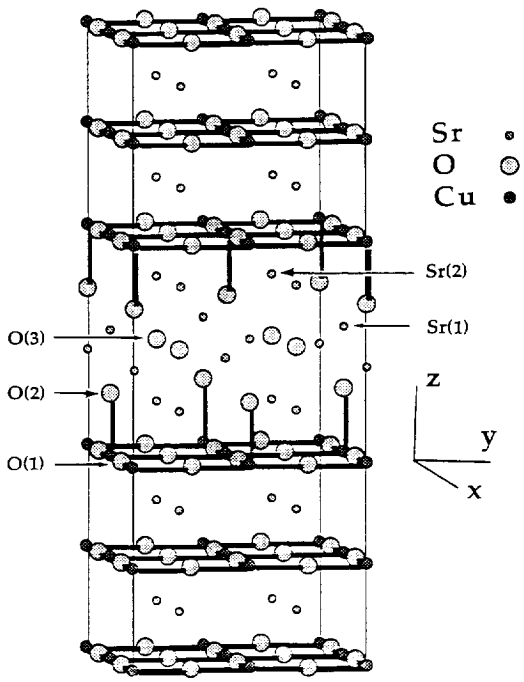

Fig. 6. Structural model for the planar defect. Three Sr–O layers replace a Sr(Ca)–CuO_2–Sr(Ca) block in an otherwise perfect infinite-layer structure. The first and third layers consist of about 50% oxygen occupancy. The middle layer strontiums are randomly staggered in response to loss of full oxygen coordination.

The atomic position of the strontium was refined by χ^2 fittings. An area of 128×80 pixel^2 in the defect region was employed to improve the statistic errors. The standard deviation used for χ^2 calculation was calibrated using the experimental images in the defect regions. Fig. 7 shows χ^2 as a function of the staggering of Sr(1) in the middle layer of $Sr_3O_{2\pm x}$ block. The distance of the staggering is measured from the middle position of the two coppers of the top and bottom CuO_2 planes of the defect model, which was taken as the zero position. As we can see, all three images have the staggering position as the minimum χ^2 value. By polynomial curve fitting these three sets of data, the minimum χ^2 are 1.95 at 0.557 Å, 1.58 at 0.653 Å and 1.65 at 0.525 Å for a, b and c respectively. Therefore the staggering atomic position of Sr(1) is optimized as 0.58 ± 0.07 Å with a 68% confidence level. It should be pointed out that the apical oxygen is correspondingly adjusted to the middle position of the copper and Sr(1) when varying the position of Sr(1), which seems justified by comparison with the apical oxygen positions in many cuprate superconductors, for instance La_2CuO_4 [12]. χ^2 values below 2 for all three focal images indicate that the structure model of planar defect is reasonable.

Fig. 8 shows the χ^2 variation as a function of the position of Sr(2) in the first and third layers

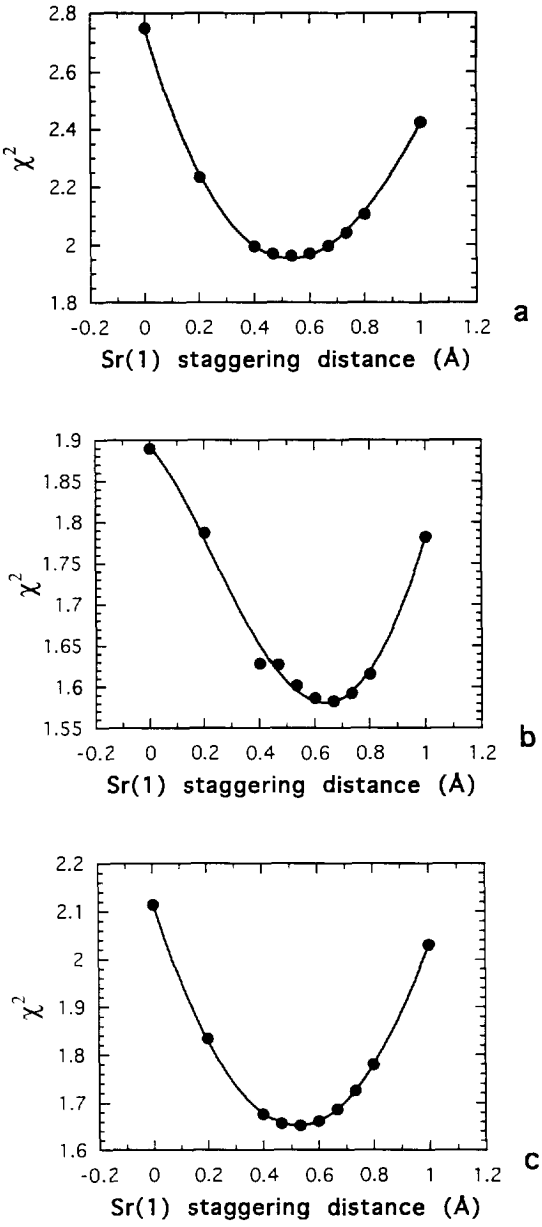

Fig. 7. χ^2 evolution as a function of staggering position of Sr(1) in the middle Sr–O layer which is calculated from the middle position of two coppers in top and bottom CuO_2 for images at defoci: (a) 0 Å, (b) −460 Å and (c) −740 Å. Sample thickness is 20 Å.

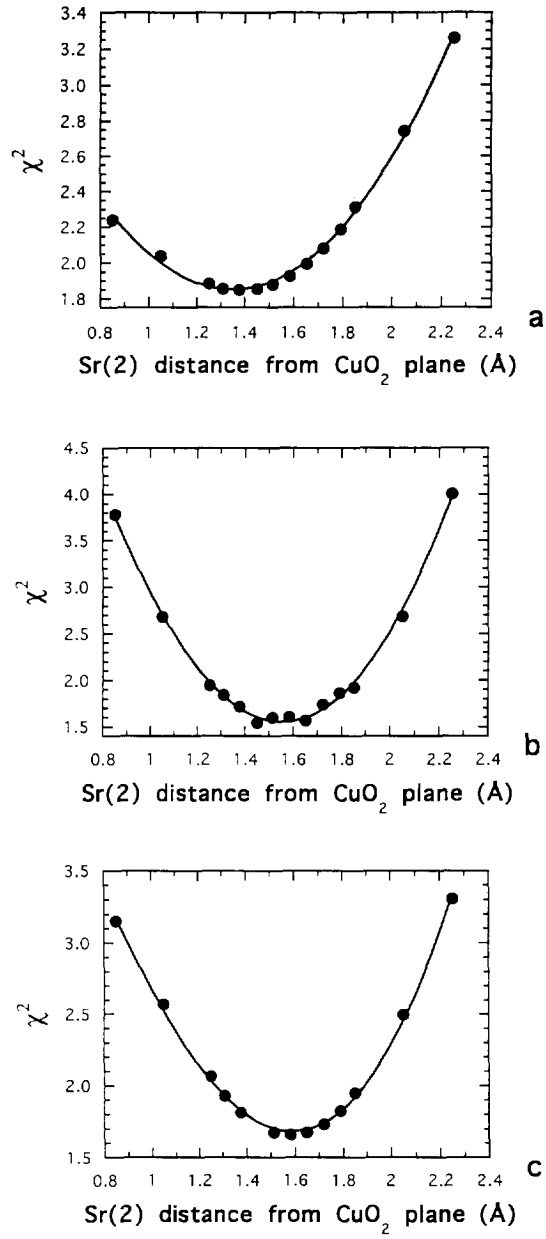

Fig. 8. χ^2 evolution as a function of the distance of Sr(2) from the CuO_2 plane for the images of defoci: (a) 0 Å, (b) −460 Å and (c) −740 Å with a sample thickness of about 20 Å.

with the Sr(1) optimized. The Sr(2) position shown in this figure is the distance of the strontium to the neighbour CuO_2 plane. Similarly, with Sr(1) staggering at the middle layer the optimized position of Sr(2) is 1.5 ± 0.12 Å with a 68% confidence level. Fig. 9 shows the χ^2 as a function of

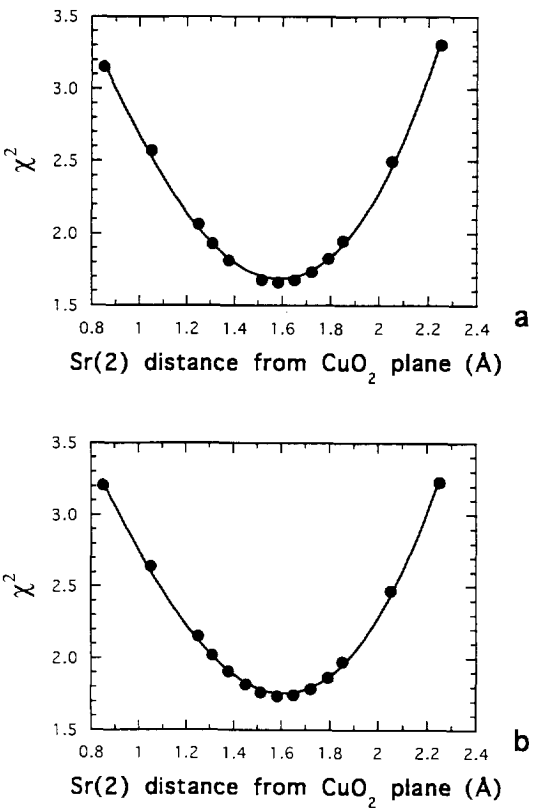

Fig. 9. Variation of χ^2 as a function of the distance of Sr(2) from the CuO_2 plane with different vibration added, 4.5 pixels for (a) and 5.4 pixels for (b), for the image with a defocus of −740 Å.

the distance of Sr(2) away from the CuO_2 plane as a function of the vibrations, vibration in Fig. 9a is 4.5 pixels (0.59 Å) and 5.4 pixels (0.70 Å) in Fig. 9b. Figs. 9a and 9b show the same evolution with the Sr(2) position. The Sr(2) position at the minimum χ^2 does not vary much, 1.61 Å for Fig. 9a and 1.59 Å for Fig. 9b. The difference is 0.02 Å and it is within the range of the error bar.

4. Discussion

From the above results the best atomic positions of the defect model are listed in Table 1. It is clear that the Sr(2) atom is closer to the CuO_2 plane than to the staggered SrO plane in the middle due to the fact that CuO_2 is a more negatively charged plane. Our model for the planar defects is a structural configuration not found in any layered cuprate compounds made under ambient condition. However, the structural similarity to the $Sr_2O_{1\pm x}$ layers in the newly discovered $Sr_{n+1}Cu_nO_{2n+1\pm x}$ compounds which are also synthesized at high pressure is intriguing. Both structures also share the interesting feature of having substantially less than full occupancy (about 50% in the present case) of the apical oxygen atoms around the copper ions. Infinite-layer systems show strong variations in the superconductivity as a function of the synthesis atmosphere, i.e. p-type with T_c up to 110 K under oxidizing conditions, n-type with T_c up to 43 K under reducing conditions. The 50% occupancy of oxygen in the defect may lead to p-type superconductivity if doped by excess oxygen ($x > 0$) or n-type superconductivity with oxygen deficiency ($x < 0$). Further quantitative comparisons of HREM images of the defect structures under oxidizing and reducing conditions might be important to understand.

It is appropriate here to make some general comments about χ^2 refinements of atomic positions from HREM images. Perhaps the most important point is recognition that the error bar of such a measurement is at least as important as the actual value. A large number of programs are available for performing non-linear least-squares fittings suitable for minimizing χ^2, which will give errors. However, many assumptions are built in

Table 1
Atomic position of the defect (unit cell for the defect is 3.9 × 3.9 × 7.4 Å^3 (xyz) and atomic positions are in fraction of the unit cell dimensions)

	Cu	O(1)	O(2)	O(2) *	O(2) *	O(3)	Sr(1) *	Sr(1) *	Sr(2)	Sr(2)
x	0	0.5	0	0	0	0.5	0	0	0.5	0.5
y	0	0	0.5	0	0	0.5	0	0	0.5	0.5
z	0	0	0	0.29	0.71	0.5	0.42	0.58	0.22	0.78

* Half occupancy.

to these, such as approximating the minimum as parabolic. A very simple demonstration of the problems with this is the fitting of the defocus near to Scherzer shown in Fig. 4b. Over a wide range of values, χ^2 is quite flat and also less than 1. This means that not only is the true error in defocus here large, but also that there is a real danger of overfitting the defocus. (This will almost certainly always be a problem when the defocus is over a pass-band for the sample, because under such conditions to first order the image is independent of defocus.) For these reasons anything less than fitting three members of a focal series is highly dubious; a simple analogy would be fitting a straight line to two points.

Also very important is proper determination of the experimental error for the intensities. The method that we have used here of looking at the local image variations should be very valid and generally applicable. As a caveat, it should be noted that the whole principle of a χ^2 minimization does assume that the experimental errors are Gaussian; if they are not then the function to be minimized (Eq. (1)) should be changed.

Acknowledgements

This research was supported by the National Science Foundation under Grant No. DMR 91-20000, through the Science and Technology Center for Superconductivity.

References

[1] D.J. Smith, W.J. de Ruijter, M.R. McCartney and J.K. Weiss, Ultramicroscopy 52 (1993) 591.
[2] A.R. Smith and L. Eyring, Ultramicroscopy 8 (1982) 65.
[3] W.E. King and G.H. Campbell, in: Atomic Scale Imaging of Surfaces and Interfaces, Eds. D. Biegelsen, D.J. Smith and S.Y. Tong, MRS Symp. Proc. 295 (1993) 83.
[4] W.E. King and B.S. Lamrer, in: Microbeam Analysis 1991, Ed. D.G. Howitt (San Francisco Press, San Francisco, 1991) p. 217.
[5] J.F. Banfield, D.R. Veblen and D.J. Smith, Am. Mineral. 76 (1991) 343.
[6] W. Dong, T. Baird, J.R. Fryer, C.J. Gilmore, D.D. MacNicol, G. Bricogne, D.J. Smith, M.A. O'Keefe and S. Hovmöller, Nature 355 (1992) 605.
[7] J.J. Hu and F.H. Li, Ultramicroscopy 35 (1991) 339.
[8] M. Azuma, Z. Hiroi, M. Takano, Y. Bando and Y. Takeda, Nature 356 (1992) 775.
[9] Z. Hiroi, M. Azuma, M. Takano and Y. Takeda, Physica C 208 (1993) 286.
[10] H. Zhang, Y.Y. Wang, H. Zhang, V.P. Dravid and L.D. Marks, P. Han, D.A. Payne, P.G. Radaelli and J.D. Jorgensen, Nature 370 (1994) 352.
[11] P. Xu, G. Jayaram and L.D. Marks, Ultramicroscopy 53 (1994) 15.
[12] J.D. Jorgensen, Jpn. J. Appl. Phys. 26, Suppl. 26-3 (1987) 2017.